Estimation of charge-ordering patterns in θ-$ET_2MM'(SCN)_4$ (MM'=RbCo, RbZn, CsZn) by reflection spectroscopy

H. Tajima and S. Kyoden
Institute for Solid State Physics, The University of Tokyo, Kashiwanoha 5-1-5, Chiba 277-8581, Japan

H. Mori and S. Tanaka
International Superconductivity Technology Center, Shinonome, Tokyo 135-0062, Japan

(Received 26 April 2000)

Temperature dependence of the polarized reflectance spectra have been measured on single crystals of θ-$ET_2MM'(SCN)_4$ (abbreviated as θ-MM'; MM'=RbCo, RbZn, and CsZn). The reflectance spectra of the θ-RbCo and θ-RbZn salts exhibit drastic change around 190 K for the samples cooled slowly ($dT/dt \sim -0.1$ K/min). This spectral change disappears for the samples cooled rapidly ($dT/dt \sim -1$ K/min). The reflectance spectra of the θ-CsZn salt exhibit Drude-like features down to 20 K. Charge-ordering patterns on these salts are deduced from the spectral analysis using the mean-field calculations.

I. INTRODUCTION

Optical spectra of molecular conductors contain a lot of information such as electron-electron correlation effects, electron-phonon interaction, etc. However, the interpretation of the optical spectra is not straightforward. Among all, the coexistence of metallic conduction and the midinfrared band (intense absorption band appearing in the midinfrared region) in one-dimensional molecular conductors has puzzled many researchers.[1] In order to explain these phenomena, the following hypotheses were recently proposed by Yamamoto *et al.*:[2]

(i) In some one-dimensional conductors, the original crystal symmetry is broken even at room temperature due to spin polarization (or charge ordering) resulting from the Coulomb repulsion.

(ii) The symmetry breaking due to the Coulomb repulsion is followed by domain formation. Electric current is carried by charged domain walls rather than by single particles.

(iii) The symmetry breaking at around room temperature is in most cases not detected by magnetic resonance studies such as NMR, since the motion of the domain wall exceeds a speed limit coming from the resonance frequency.

(iv) The midinfrared band is essentially the interband transition within spin-polarized (or charge-ordered) domains.

To examine these hypotheses, the author (H.T.) calculated the optical conductivity spectrum of a one-dimensional quarter-filled molecular conductor by the use of the mean-field approximation, and showed that the mean-field approximation gives a qualitative but comprehensive interpretation of the midinfrared band.[3]

The midinfrared band is not restricted to quasi-one-dimensional conductors. Some of two-dimensional molecular conductors, which fall into an insulating state at a low temperature, also exhibit this band.[1,4] Thus, it is of interest to examine whether or not the same procedure of the analysis is applicable to two-dimensional molecular conductors. In this context, we have done spectroscopic study for θ-$ET_2MM'(SCN)_4$ (abbreviated as θ-MM'; MM'=RbCo, RbZn, and CsZn).

θ-MM' salts (M=Rb, Tl, Cs, M'=Co, Zn) are a series of molecular conductors intensively studied by Mori and coworkers.[5–9] These salts have crystal structures similar to θ-ET_2I_3, which exhibits superconductivity below 3.6 K under ambient pressure.[10] Although Co^{2+} in the M'=Co salts has the local magnetic moment with $S=3/2$, the interaction between the local magnetic moment and conduction electrons derived from π-MO of ET is quite weak.[5,8] Therefore, the electrical behavior of the Co salt is essentially the same as that of the corresponding Zn-substituted salts where no local magnetic moment is included.[6] Figure 1 shows the crystal structure of the θ-RbCo salt at room temperature.[9] Within a framework of the tight-binding model, the band structures of the θ-type molecular conductors are determined by the two transfer integrals t_p and t_c, where the subscripts ''p'' and ''c'' denote the overlapping mode shown in Fig. 1. The shape of the Fermi surface given by the tight-binding calculation is reported to be a tube having an elliptical cross section for θ-MM' salts (M=Rb, Tl, Cs, M'=Co, Zn).[6,9]

Electrical resistivity of the θ-RbCo and θ-RbZn salts is

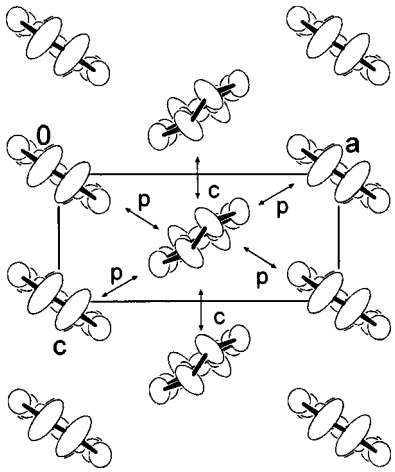

FIG. 1. Crystal structure of the θ-RbCo salt at room temperature (Ref. 9). The two kinds of overlapping modes between neighboring molecules are denoted by p and c in the figure.

almost constant (metallic) from room temperature down to 190 K. Below 190 K, the resistivity abruptly increases, and the salts fall into an insulating state.[6] The magnetic susceptibility below and above 190 K is almost continuous and does not exhibit any anomalous feature related to the phase transition.[6] On further lowering the temperature, the π-electron system of the θ-RbCo and θ-RbZn salts falls into the spin-Peierls state below 20 K.[6] X-ray crystal structural analysis has revealed that the metal-insulator transition around 190 K is accompanied by the dimerization along the c axis.[9] Interestingly, the above-mentioned behavior below 190 K disappears, when samples are cooled rapidly ($dT/dt \geqslant 1$ K/min): the magnetic susceptibility of the samples cooled in this condition exhibits the Curie-Weiss tail below 90 K and does not indicate any symptom of the spin-Peierls transition.[11] In the following, we refer this state below 190 K as the quenched state (Q state), and the other state below 190 K—the dimerized state reached when samples are cooled slowly—as the relaxed state (R state).

The electrical resistivity of the θ-CsZn salt is metallic down to 20 K and then increases. In this salt an increase of susceptibility below 20 K is observed.[6,12] The principal axis of the EPR g tensor was recently reported to rotate with lowering the temperature.[13] The spin-density-wave formation is suggested as an origin of this metal-insulator transition by the specific-heat measurements.[14]

In this paper, we describe the results of the reflectivity measurements for the θ-RbCo, θ-RbZn, and θ-CsZn salts and show the conductivity spectra experimentally obtained. Then we present the conductivity spectra given by the mean-field calculation. Finally, by comparing the features of the observed spectra with those of the calculated spectra, we deduce the charge-ordering patterns of the θ-RbCo, θ-RbZn, and θ-CsZn salts.

II. EXPERIMENTAL

Single crystals of the θ-RbCo, RbZn, and CsZn salts were synthesized by the method described elsewhere.[6,9] Reflectance spectra were measured by the use of a Fourier transform infrared (FTIR) microspectrophotometer (Jasco FTIR 8900μ) from 650 to 5000 cm^{-1}, and the Olympus MMSP-RK microspectrophotometer from 5000 to 25000 cm^{-1}. Samples were cooled by a cryostat manufactured at Oxford Ltd. (CF1104). For the θ-RbCo and θ-RbCo salts, the two different cooling rates—0.1 and 1 K/min—were chosen between 200 and 180 K to bring them into the R and Q states, respectively. The effect of the heating cycle on the spectra was examined and concluded to be negligible in this experiment. The Kramers-Kronig transformation was performed by extrapolating the reflectance data to zero wave number. The shapes of the obtained conductivity spectra were little affected by the method of extrapolation except for the spectra of the θ-CsZn salt below 200 K.

III. RESULTS

Figure 2 shows the reflectance spectra of the θ-RbCo, θ-RbZn, and θ-CsZn salts on the (010) crystal surface at room temperature. In these measurements, we have chosen the directions of the polarization where the reflectivity takes the maximum and the minimum values. These directions coincide with the a and c axes for all the three salts as expected from the crystal symmetry. The dispersion around 1300 cm^{-1} is attributable to a_g molecular vibration mode induced by the electron-molecular-vibration coupling. The sharp peak around 2100 cm^{-1} is attributable to the C═N stretching mode of SCN$^-$. The reflectance spectra of the θ-RbCo and θ-RbZn salts are quite similar to each other. This similarity is consistent with the unified phase diagram proposed by Mori for the θ-type salts.[6] By applying the Drude-Lorentz model to the observed spectra, we have found that the spectra of the θ-CsZn salt contains the Drude contribution, which comes from electronic transition having zero (or very small) excitation energy, while such contribution is absent (or negligibly small) in the spectra of the θ-RbCo and θ-RbZn salts.

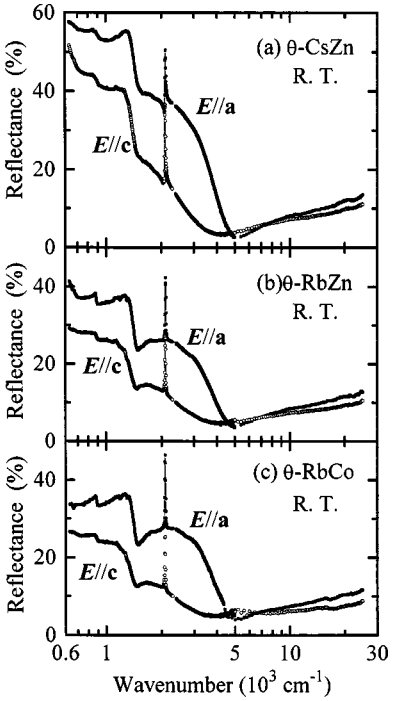

FIG. 2. Reflectance spectra of the (a) θ-CsZn, (b) θ-RbZn, and (c) θ-RbCo salts at room temperature.

Figure 3 shows the optical conductivity spectra obtained from the reflectance spectra shown in Fig. 2 through the Kramers-Kronig transformation. As expected from the shape of the reflectance spectra, the optical gap is absent in the spectra of the θ-CsZn salt. On the contrary, the conductivity spectra of the θ-RbCo and θ-RbZn salts take a broad maximum around 2500 cm^{-1}. Here we should note that the only allowed electronic transition in the simple tight-binding model of the θ-type salts is the intraband transition which gives the Drude contribution to the spectra.[4,15] Thus the deviation from the Drude-type shape of the spectra in the θ-RbCo and θ-RbZn salts indicates breakdown of the simple tight-binding picture. This will be discussed in the later sections.

Figure 4 shows the temperature dependence of the reflectance spectra of the θ-RbCo salt. We have obtained the two kinds of spectra—the spectra in the Q and R states—below 190 K. The spectral features of the Q state are similar to those of the metallic state above 190 K, but completely different from those of the R state. Thus we conclude that the Q

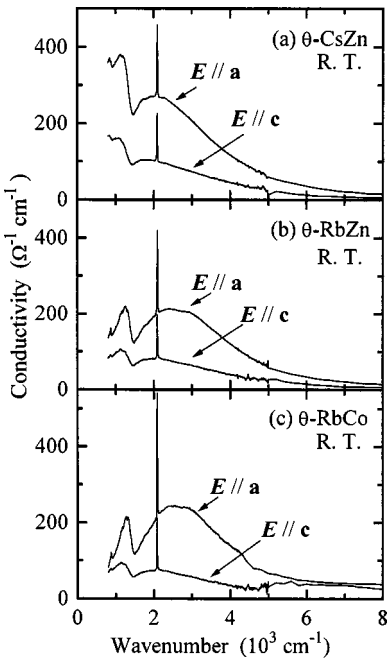

FIG. 3. Conductivity spectra of the (a) θ-CsZn, (b) θ-RbZn, and (c) θ-RbCo salts at room temperature, obtained from the reflectance spectra shown in Fig. 2 through Kramers-Kronig transformation.

state is a supercooled state of the high-temperature metallic phase, while the *R* state is a different phase. This conclusion is consistent with the EPR experiments by Nakamura *et al.*[11]

Figure 5 shows the optical conductivity spectra obtained through the Kramers-Kronig transformation from the reflectance spectra of Fig. 4. The spectra in the *Q* state and the

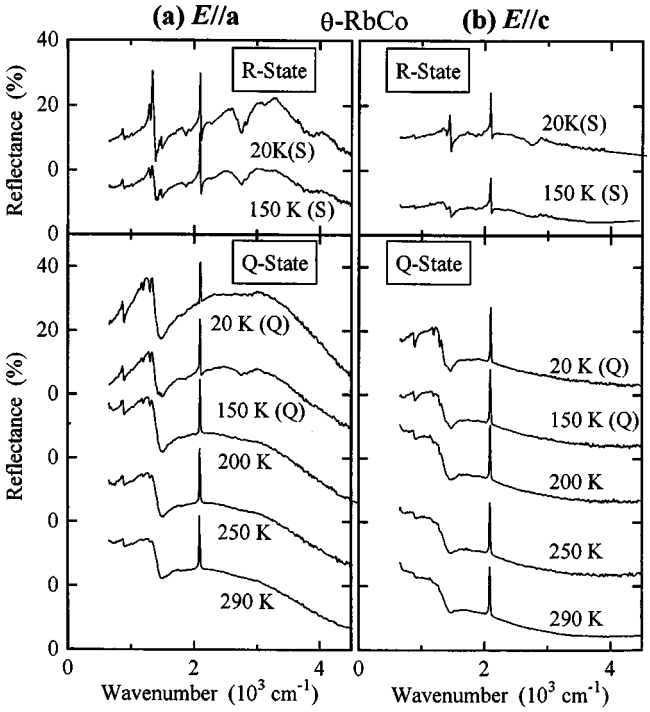

FIG. 4. Temperature dependence of the infrared reflectance spectra of the θ-RbCo salt for the (a) $\mathbf{E}\|\mathbf{a}$ and (b) $\mathbf{E}\|\mathbf{c}$ polarizations. The notations (*Q*) and (*R*) indicate the *Q* and *R* states, respectively. Note the scale offset between different spectra.

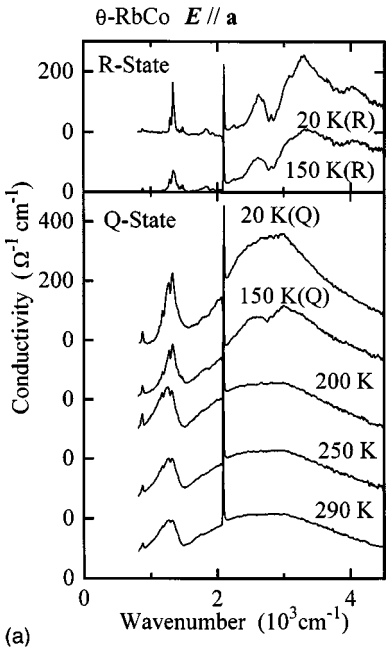

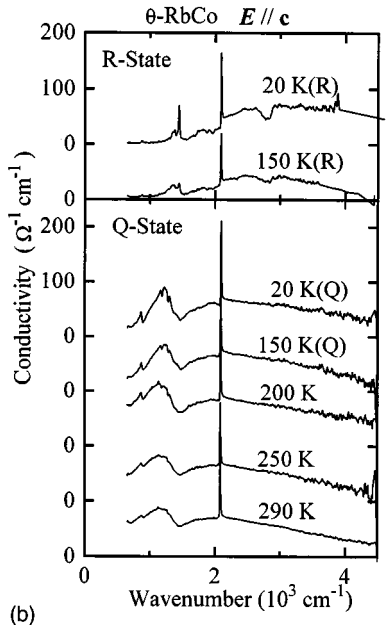

FIG. 5. Temperature dependence of the optical conductivity spectra of the θ-RbCo salt for the (a) $\mathbf{E}\|\mathbf{a}$ and (b) $\mathbf{E}\|\mathbf{c}$ polarizations. The notations (*Q*) and (*R*) indicate the *Q* and *R* states, respectively. Note the scale offset between different spectra.

metallic state above 190 K exhibit a single broad absorption band around 3000 cm^{-1}. On the other hand, the spectra in the *R* state exhibit three absorption bands above 2000 cm^{-1}.

Figure 6 shows the temperature dependence of the reflectance spectra of the θ-CsZn salt. The spectral shape exhibits a feature of metallic dispersion down to 20 K. This salt is reported to undergo a metal-insulator transition at 20 K. However, we could not cool the sample below 20 K in the present measurements. Therefore, spectral change (if any) associated with this metal-insulator transition has not been investigated in the present study.

Figure 7 shows the optical conductivity spectra obtained through the Kramers-Kronig transformation from the reflec-

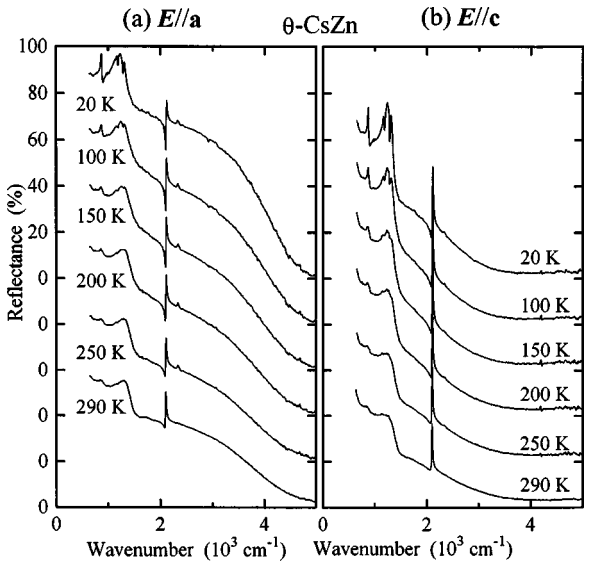

FIG. 6. Temperature dependence of the infrared reflectance spectra of the θ-CsZn salt for the (a) $\mathbf{E}\|\mathbf{a}$ and (b) $\mathbf{E}\|\mathbf{c}$ polarizations. Note the scale offset between different spectra.

tance spectra shown in Fig. 6. Although the conductivity spectra below 200 K have been affected a little by the extrapolation used in the Kramers-Kronig transformation, the conductivity spectra do not exhibit a gap for any attempted extrapolations. This is consistent with the Drude-like feature of the reflectance spectra. Therefore, we conclude that there exists an intense absorption band with extremely small (or zero) excitation energy, although we cannot assign whether or not this band is due to the intraband transition. Another important feature of the conductivity spectra is a broad absorption band around 2000 cm^{-1}. This band is obscure around room temperature and becomes intense with lowering the temperature. A similar absorption band is also observed in θ-ET_2I_3.[15] However, the spectral intensity of the absorption band in this salt is much larger than that of the corresponding band in θ-ET_2I_3. Later in this paper, we will discuss the origin of this transition in detail.

IV. DISCUSSION

A. Theoretical calculation of the conductivity spectra

One of the problems in the mean-field approximation is multivaleny of the self-consistent-field (SCF) equation. In the normal mean-field procedures, a SCF solution which has the lowest energy is chosen as the most plausible solution for a given sets of parameters. However, the choice of the SCF solution in this procedure is often a subtle problem, since the energy differences between different SCF solutions are not always large enough. This problem becomes serious as we increase the number of the mean-field parameters.

In this paper, we propose that the SCF solution appropriate to the observed state may be determined by the spectral analysis. The point of this method is to derive some relation between the spectral feature and a certain SCF solution by calculating the optical conductivity spectra on the basis of the mean-field approximation. With the help of the relation thus obtained, we deduce the SCF solution appropriate to the

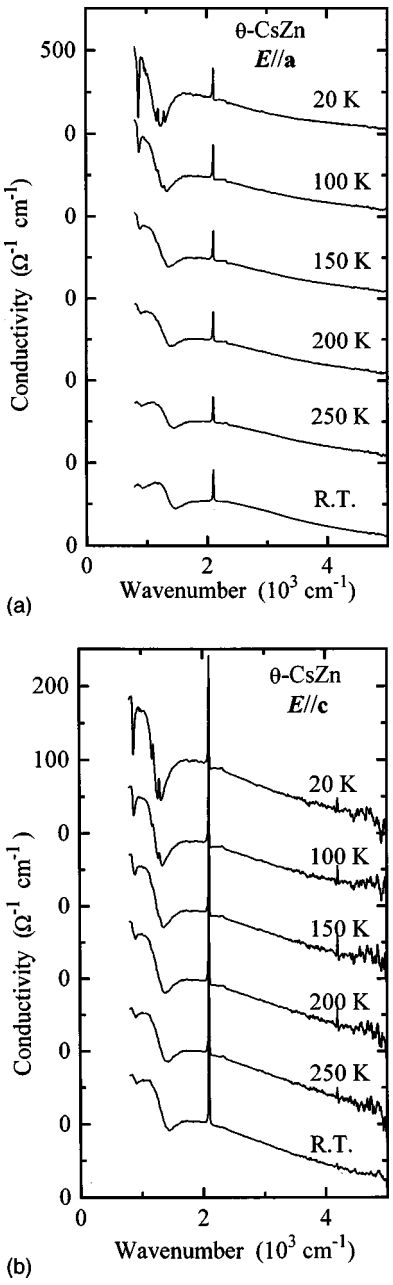

FIG. 7. Temperature dependence of the optical conductivity spectra of the θ-CsZn salt for the (a) $\mathbf{E}\|\mathbf{a}$ and (b) $\mathbf{E}\|\mathbf{c}$ polarizations. Note the scale offset between different spectra.

observed optical conductivity spectra. Once the SCF solution is determined by this method, we can find out the charge-ordering patterns, degree of spin-polarization, etc., because such information is included in the SCF solution. Here we should note that the spectral calculation based on the mean-field approximation has been previously carried out for one-dimensional quarter-filled conductors by the author (H.T.).[3] The calculated conductivity spectra are consistent with those experimentally obtained, although the spectral change associated with the phase transition from an antiferromagnetic state to a charge-ordered state has been found to be negligibly small in the case of the one-dimensional quarter-filled conductors.

In this calculation, we assume an extended Hubbard Hamiltonian,

$$H=\sum_{ijpq\sigma}(t_{ijpq}c^{+}_{ip\sigma}c_{jq\sigma}+\text{c.c.})+\sum_{ijpq}V_{ijpq}n_{ip}n_{jq}+U\sum_{i}n_{ip\uparrow}n_{ip\downarrow}, \quad (1)$$

where $c^{+}_{ip\sigma}$, $c_{ip\sigma}$ are creation and annihilation operators for an electron with spin σ ($=\uparrow$ or $\downarrow$) on pth molecular site in the ith cell. We reduce this extended Hubbard Hamiltonian into the effective mean-field Hamiltonian

$$H_{\text{mean}}=\sum_{ijpq\sigma}(t_{ijpq}c^{+}_{ip\sigma}c_{jq\sigma}+\text{c.c.})+\sum_{ijpq}V_{ijpq}(\langle n_{ip}\rangle n_{jq}+\langle n_{jq}\rangle n_{ip}-\langle n_{ip}\rangle\langle n_{jq}\rangle)+U\sum_{i}(\langle n_{ip\uparrow}\rangle n_{ip\downarrow}+\langle n_{ip\downarrow}\rangle n_{ip\uparrow}-\langle n_{ip\uparrow}\rangle\langle n_{ip\downarrow}\rangle) \quad (2)$$

in a similar manner reported by Seo[16] and Seo-Fukuyama.[17] The choice of the unit cell is crucial in this calculation. For the θ-type molecular conductors, Seo has derived many kinds of SCF solutions by assuming a unit cell containing eight molecules. In our present calculation we assume $2\mathbf{c}\times\mathbf{a}$ and $2\mathbf{c}\times(\mathbf{c}+\mathbf{a})$ unit cells, both of which contain four molecules. The assumed unit cell are enough for the spectral analysis, although some of the SCF solutions appearing in Seo's study are missing in our calculation.

This calculation is essentially a band structure calculation where the unit cell contains four molecules. Therefore, the highest occupied molecular orbital, which forms the conduction band, splits into four bands in this approximation. We number them from 1 to 4 in the order of energy, i.e., band 1 has the lowest energy and so on.

After we evaluate the mean-field parameters by means of the SCF calculation, we calculate the optical conductivity spectra by using

$$\sigma_{\alpha}(\omega)=\text{Re}\left\{\frac{1}{i\Omega\hbar^{3}}\sum_{n}\frac{\omega}{\omega_{n0}}\frac{2[H_{\text{mean}},P_{\alpha}]_{0n}[H_{\text{mean}},P_{\alpha}]_{n0}}{(\omega^{2}-\omega^{2}_{n0}-i\omega\Gamma)}\right\}. \quad (3)$$

Here $\mathbf{P}$ is a dipole operator, defined as

$$\mathbf{P}=e\sum_{i}\mathbf{R}_{i}c^{+}_{i\sigma}c_{i\sigma}, \quad (4)$$

and Γ is the relaxation rate.[3,18]

In the following calculation, we assume Γ to be 0.1 eV, and use transfer integrals—$t_c=-0.033$ eV and $t_p=0.099$ eV—which were obtained for the θ-RbCo salt at room temperature.[9] We assume the Coulomb-repulsion parameters, $U=0.8$ eV, $V_p=0.1$ eV, and V_c to be a adjustable parameter ranging from $V_c=0$ eV to $V_c=0.3$ eV. (As for subscripts ''p'' and ''c,'' see the overlapping mode of molecules shown in Fig. 1.) We have determined the Coulomb-repulsion parameters so that a phase transition occurs in the calculation. Although some ambiguity is inevitable in the above choice of the parameters, it is not serious in the following discussion. Here we should note that the value of $U-V_p=0.7$ eV is consistent with $U_{\text{eff}}(=U-V)=0.7$ eV, which was obtained for ET·$HgBr_3$ based on optical measurements.[19]

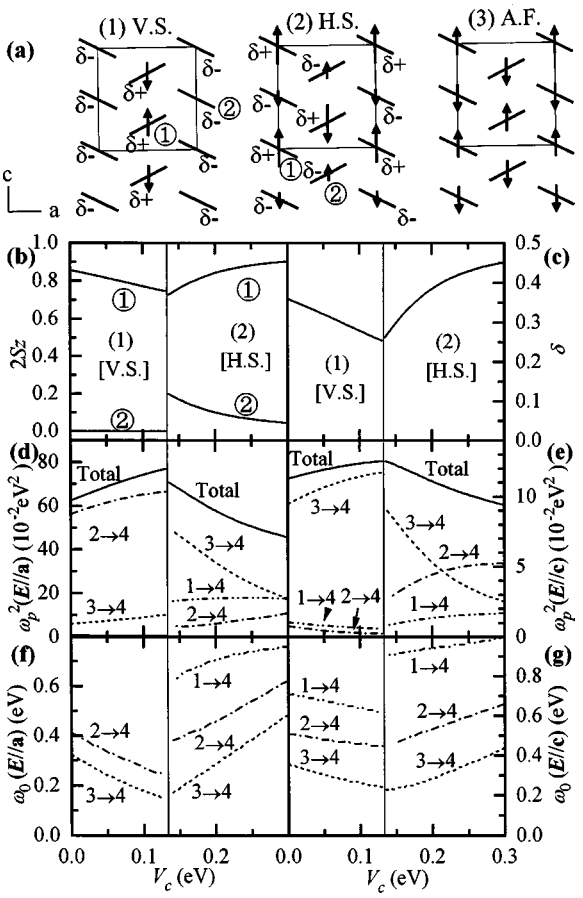

FIG. 8. Summaries of the mean-field calculations for the $2\mathbf{c}\times\mathbf{a}$ lattice. In this calculation, $t_c=-0.033$ eV, $t_p=0.099$ eV, $U=0.8$ eV, and $V_p=0.1$ eV are assumed: (a) the schematic charge-ordering patterns in the SCF solutions; (b) net spin on the sites ① and ② [see the definition shown in (a)]; (c) degree of charge transfer from site ① to site ②; (d) the intensity of the absorption band in the $\mathbf{E}\|\mathbf{a}$ conductivity spectra; (e) the intensity of the absorption band in the $\mathbf{E}\|\mathbf{c}$ conductivity spectra; (f) the peak positions of the $n\rightarrow 4$ ($n=1,2,3$) optical transitions in the $\mathbf{E}\|\mathbf{a}$ conductivity spectra; (g) the peak positions of the $n\rightarrow 4$ ($n=1,2,3$) optical transitions in the $\mathbf{E}\|\mathbf{c}$ conductivity spectra.

Figure 8(a) shows the schematic patterns of charge ordering in the SCF solutions obtained for the $2\mathbf{c}\times\mathbf{a}$ structure. The solutions are denoted by (1) VS (vertical stripe), (2) HS (horizontal stripe), and (3) AF (antiferromagnetic). In the present sets of parameters, the AF solution is metastable and the most stable SCF solution is (1) VS for $0\text{ eV}<V_c<0.13$ eV, and (2) HS for $0.14\text{ eV}<V_c<0.3$ eV. However, the energy differences among these solutions are quite small. Thus we consider the possibility that the AF state is realized in the actual system. In the following calculations shown in Figs. 8(b)–8(g) and Figs. 10(b)–10(g) we only show the results of the calculation for the most stable SCF solutions, while the spectral calculation for the metastable AF solution will be described in Fig. 11.

Figures 8(b) and 8(c) show net spin $2S_z$ on the two sites (①, ②), and degree of charge disproportionation δ. Figures 8(d) and 8(e) show the total spectral intensity ω_p^2 defined by

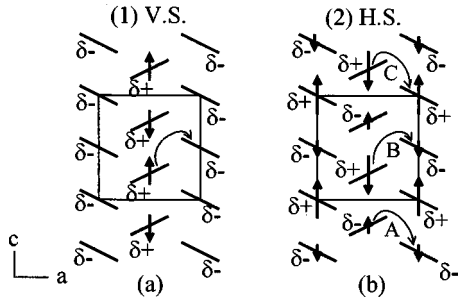

FIG. 9. A schematic explanation for the spectral difference between the HS and VS states. The possible excitation configuration is only one for the VS ground state (a), while it is three for the HS ground state (b).

$$\omega_p^2 = 8\int_0^\infty \sigma(\omega)d\omega, \tag{5}$$

and its fraction due to the $m \rightarrow n$ interband transition for the $\mathbf{E}\|\mathbf{a}$ and $\mathbf{E}\|\mathbf{c}$ polarizations, respectively. Figures 8(f) and 8(g) show the peak positions of the $m \rightarrow n$ interband transition for the $\mathbf{E}\|\mathbf{a}$ and $\mathbf{E}\|\mathbf{c}$ polarizations, respectively. The intraband transition does not appear in both (1) VS and (2) HS solutions.

As can be seen from the spectral intensity shown in Figs. 8(d) and 8(e) the spectral shape in the (1) VS solution is almost determined by the $2 \rightarrow 4$ interband transition for the $\mathbf{E}\|\mathbf{a}$ polarization, and the $3 \rightarrow 4$ interband transition for the $\mathbf{E}\|\mathbf{c}$ polarization. [See the left half of Figs. 8(d) and 8(e).] Thus the single-peaked shape is expected for the optical conductivity spectra in the (1) VS solution. On the contrary, the spectral line shape in the (2) HS state is determined by a combination of the $3 \rightarrow 4$, $2 \rightarrow 4$, and $1 \rightarrow 4$ interband transitions. [See the right half of Figs. 8(d) and 8(e).] Therefore, the triple-peaked line shape of the conductivity spectra is expected for the (2) HS solution.

Figure 9 shows a schematic explanation for the spectral difference between the HS and VS states. The point of this explanation is to neglect the transfer integral along c axis, t_c. Under this assumption, the possible excitation configuration is only one for the VS ground state [Fig. 9(a)], while it is three ($A \sim C$) for the HS ground state [Fig. 9(b)]. Therefore, the conductivity spectra in the VS state exhibit single-peaked feature, while the spectra in the HS state exhibit triple-peaked feature.

Figure 10 shows the spectral feature calculated for the $2\mathbf{c} \times (\mathbf{a}+\mathbf{c})$ lattice. In this choice of lattice, we obtain three SCF solutions corresponding to the ordering patterns denoted in Fig. 10(a) by (4) VS, (5) DS (diagonal stripe), and (6) AF. In the $\mathbf{E}\|\mathbf{a}$ spectra of the (4) VS solution, the spectral intensities of the $3 \rightarrow 4$ and $2 \rightarrow 4$ optical transitions are comparable. [See the left half of Fig. 10(d).] However, the peak positions of the two transitions are close to each other. [See the left half of Fig. 10(f).] Therefore, peak splitting does not occur unless the spectra have narrow line widths. In the $\mathbf{E}\|\mathbf{c}$ spectra of the (4) VS solution, the spectral feature is determined by the $3 \rightarrow 4$ transition [see left halves of Figs. 10(e) and 10(g)] as well as in the $\mathbf{E}\|\mathbf{c}$ spectra of the (1) VS solution in the $2\mathbf{c} \times \mathbf{a}$ lattice. Therefore, single-peaked shape is expected. In the spectra of the (5) DS solution, the spectral

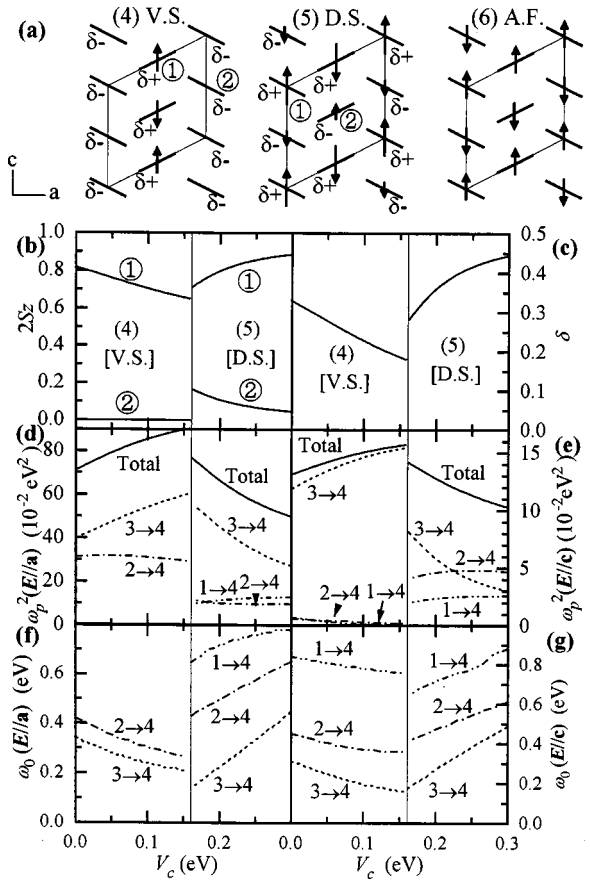

FIG. 10. Summaries of the mean-field calculations for the $2\mathbf{c} \times (\mathbf{a}+\mathbf{c})$ lattice. In this calculation, $t_c = 0.033$ eV, $t_p = 0.099$ eV, $U = 0.8$ eV, and $V_p = 0.1$ eV are assumed: (a) the schematic charge-ordering patterns in the SCF solutions; (b) net spin on the sites ① and ② [see the definition shown in (a)]; (c) degree of charge transfer from site ① to site ②; (d) the intensity of the absorption band in the $\mathbf{E}\|\mathbf{a}$ conductivity spectra; (e) the intensity of the absorption band in the $\mathbf{E}\|\mathbf{c}$ conductivity spectra; (f) the peak positions of the $n \rightarrow 4$ ($n = 1,2,3$) optical transitions in the $\mathbf{E}\|\mathbf{a}$ conductivity spectra; (g) the peak positions of the $n \rightarrow 4$ ($n = 1,2,3$) optical transition in the $\mathbf{E}\|\mathbf{c}$ conductivity spectra.

intensity of the $3 \rightarrow 4$, $2 \rightarrow 4$, and $1 \rightarrow 4$ interband transitions are comparable to each other. [See the right halves of Figs. 10(d) and 10(e).] Thus the spectra exhibit triple-peaked feature likewise the spectra of the (2) HS solution in the $2\mathbf{c} \times \mathbf{a}$ lattice.

Figure 11 shows optical spectra for the typical SCF solutions given by the mean-field calculations. Here the solution denoted by ''normal metal'' is the state where neither charge ordering nor spin polarization exists. The spectra shown in Figs. 11(d) and 11(h) are the optical spectra for the AF solutions in the $2\mathbf{c} \times \mathbf{a}$ and $2\mathbf{c} \times (\mathbf{a}+\mathbf{c})$ lattices [solutions (3) and (6) in Figs. 8(a) and 10(a), respectively]. These solutions are metastable in the calculations of Figs. 8 and 10. For these solutions, the Fermi surface still exists as well as the normal metal solution. Therefore, the Drude-type intraband transition appears. Figure 11(e) shows the optical spectra calculated for the HS-type solution derived from the transfer integrals of the θ-RbCo salt at 7 K. The spectra exhibit triple-peaked feature similar to the spectra shown in Figs. 11(c) and 11(g).

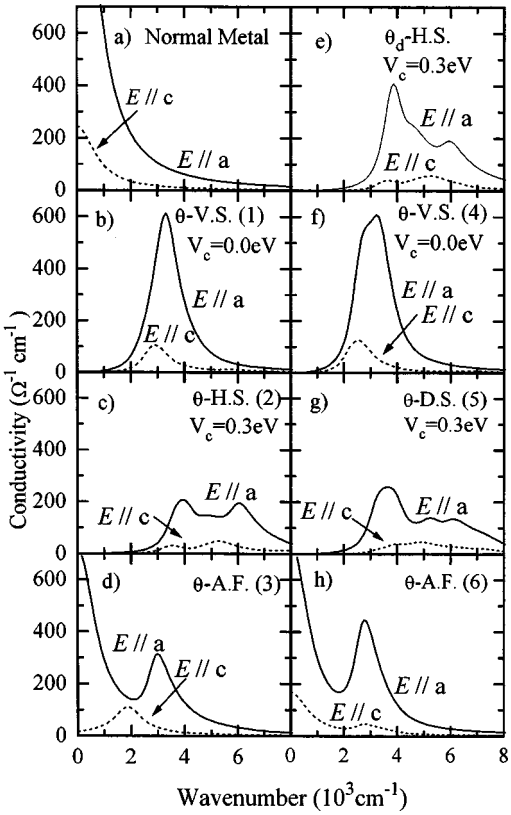

FIG. 11. Optical conductivity spectra calculated for the typical SCF solutions given below: (a) ''normal metal'' solution (the solution where neither charge ordering nor spin polarization exists); (b) VS solution in the $2\mathbf{c}\times\mathbf{a}$ lattice; (c) HS solution in the $2\mathbf{c}\times\mathbf{a}$ lattice; (d) AF solution in the $2\mathbf{c}\times\mathbf{a}$ lattice; (e) HS solution in the dimerized θ structure; (f) VS solution in the $2\mathbf{c}\times(\mathbf{a}+\mathbf{c})$ lattice; (g) DS solution in the $2\mathbf{c}\times(\mathbf{a}+\mathbf{c})$ lattice; (h) AF solution in the $2\mathbf{c}\times(\mathbf{a}+\mathbf{c})$ lattice. In this calculation, $t_c=-0.033$ eV, $t_p=0.099$ eV, $U=0.8$ eV, and $V_p=0.1$ eV are assumed except for (e). In the case of (e), the transfer integrals determined for the θ_d-RbCo salt at 7 K are assumed (Ref. 9).

B. Charge-ordering patterns in the θ-type salts

In the following, we deduce the charge-ordering patterns by comparing the conductivity spectra experimentally obtained and those calculated by means of the mean-field approximation. Although our calculations do not consider the exciton effects, a qualitative discussion is still possible because spectral difference between the VS and HS is quite large.

1. θ-RbZn and θ-RbCo salts (T<190 K: R state)

Three peaks appear in the optical conductivity of these salts (top of Fig. 5). This feature is consistent with the spectra shown in Figs. 11(c), 11(e), and 11(g). Since the DS order is not plausible in the dimerized state below 190 K, we conclude that *there is HS order in the R state of the θ-RbZn and θ-RbCo salts*. A similar conclusion has been obtained by Chiba *et al.* on the basis of NMR experiments.[20] Although consistency between the calculated and the observed spectra is not complete, this may be attributable to the exciton effects, which have not been considered in the present study. According to similar calculations for a one-dimensional quarter-filled conductor, the exciton effect becomes large as the degree of charge separation increases.[3]

2. θ-RbZn and θ-RbCo salts (T>190 K)

The spectral features of these salts (bottom of Fig. 5) are quite similar to those of Figs. 11(b) and 11(f). Thus we conclude that *there is VS order in these salts above 190 K*. One may consider that this conclusion is inconsistent with the electrical behavior, in which the resistivity is almost constant above 190 K, because the Fermi surface does not exists in the VS state. However, this inconsistency is solved by assuming the hypotheses (ii) and (iii) described in the introduction. We would like to emphasize that there are two degenerate charge-ordered states with the VS order in the θ-type structure, and such degeneracy is necessary for the domain motion assumed in the hypothesis.

If we accept the above-mentioned conclusion described for the θ-RbZn and θ-RbCo salts, the metal-insulator transition around 190 K is accompanied by the change of charge-ordering patterns from the VS order to the HS order. Since the freedom of the spin is conserved in both the VS and HS states [see $2S_z$ in Fig. 8(b)], we may expect that the susceptibility is approximately continuous below and above the phase-transition temperature. We consider that this scenario well explains the phase transition at 190 K in the θ-RbZn and θ-RbCo salts.

3. θ-RbZn and θ-RbCo salts (T<190 K: Q state)

From the spectral feature (Fig. 5), we conclude that *there is VS order in this state as well as T>190 K.* Although the VS state deduced in this study has not been reported in other experiments, this may be explained by considering that the dynamical motions of the stripe prevent the detection of the VS order.

4. θ-CsZn (T≥20 K)

The optical conductivity spectra of this salt exhibit the Drude-like feature and a broad absorption band around 2000 cm^{-1}. The latter component becomes remarkable with lowering the temperature. These spectral features are consistent with the calculated spectra shown in Figs. 11(d) and 11(h). Thus we conclude that *charge disproportionation in θ-CsZn is absent (or negligibly small)* and that *the broad absorption band around 2000 cm^{-1} originates from the fluctuation of the AF order*. This seems to be consistent with anomalous temperature dependence of T_1^{-1} observed in ^{1}H-NMR experiments.[13]

V. SUMMARY AND CONCLUSION

In the present study, we have measured the reflectance spectra of the θ-type ET salt. We have found (i) the optical conductivity spectra of the θ-CsZn salt is Drude-like down to 20 K; (ii) the spectra of the θ-RbZn and θ-RbCo salts exhibit a drastic change around 190 K, when samples are cooled down slowly; (iii) the spectral change described in (ii) is absent for samples cooled down rapidly. We have calculated optical conductivity spectra on the basis of the mean-field approximation applied to the extended Hubbard Hamiltonian. By comparing the calculated and observed spectra of

the optical conductivity, we have deduced the charge-ordering patterns of the θ-RbZn, θ-RbCo, and θ-CsZn salts. We have concluded that the phase transitions around 190 K in the θ-RbZn and θ-RbCo salts are attributable to the first-order transition from the VS state to the HS state, and that the charge disproportionation is absent (or negligibly small) in the θ-CsZn salt above 20 K. The analysis performed in this study is based on the hypotheses (i)–(iv) described in the introduction. Although these hypotheses have not yet been proved, the conclusions obtained in this study seem to be consistent with other experimental results. We consider that these hypotheses are keys to understanding the electron-electron correlation phenomena in low-dimensional conductors. In this context, it is interesting to analyze the optical conductivity spectra of other molecular conductors and inorganic conductors using the same method of the spectral analysis as that described in this article. Such studies are now in progress.

ACKNOWLEDGMENTS

We are greatly indebted to T. Mori for carefully reading the manuscript and helpful discussions. We are grateful to T. Nakamura for giving us crystals of the θ-CsZn salt and for a critical reading of the manuscript, and to N. Hanasaki, T. Yamamoto, and H. Seo for valuable discussions. We would like to thank J. Yamaura for the determination of the crystal axes. This work was supported by Grants-in-Aid for Scientific Research (No. 11136211 and No. 10640555) from the Ministry of Education, Science and Culture, Japan. Part of this work was performed using facilities in the Spectroscopy Laboratory, the Material Design and Characterization Laboratory, ISSP.

[1] For example, see C. S. Jacobsen, in *Semiconductors and Semimetals*, edited by E. Conwell (Academic, London, 1988), Vol. 27, Chap. 5.
[2] T. Yamamoto, H. Tajima, J. Yamaura, S. Aonuma, and R. Kato, J. Phys. Soc. Jpn. **68**, 1384 (1999).
[3] H. Tajima, Solid State Commun. **113**, 279 (2000).
[4] H. Kuroda, K. Yakushi, H. Tajima, A. Ugawa, M. Tamura, Y. Okawa, A. Kobayashi, R. Kato, H. Kobayashi, and G. Saito, Synth. Met. **27**, A491 (1988).
[5] H. Mori, S. Tanaka, and T. Mori, J. Phys. I **6**, 1987 (1996).
[6] H. Mori, S. Tanaka, and T. Mori, Phys. Rev. B **57**, 12 023 (1998).
[7] H. Mori, S. Tanaka, T. Mori, and H. Maruyama, Bull. Chem. Soc. Jpn. **68**, 1137 (1995).
[8] H. Mori, S. Tanaka, and T. Mori, Mol. Cryst. Liq. Cryst. Sci. Technol., Sect. A **284**, 15 (1996).
[9] H. Mori, S. Tanaka, T. Mori, A. Kobayashi, and H. Kobayashi, Bull. Chem. Soc. Jpn. **71**, 797 (1998).
[10] H. Kobayashi, R. Kato, A. Kobayashi, Y. Nishio, K. Kajita, and W. Sasaki, Chem. Lett. **1986**, 789 (1986).
[11] T. Nakamura, W. Minagawa, R. Kinami, Y. Konishi, and T. Takahashi, Synth. Met. **103**, 1898 (1999).
[12] T. Nakamura, R. Kinami, W. Minagawa, T. Takahashi, H. Mori, S. Tanaka, and T. Mori, Mol. Cryst. Liq. Cryst. Sci. Technol., Sect. A **285**, 57 (1996).
[13] T. Nakamura, W. Minagawa, R. Kinami, and T. Takahashi, J. Phys. Soc. Jpn. **69**, 504 (2000).
[14] Y. Nishio, Y. Nihei, M. Tamura, K. Kajita, T. Nakamura, and T. Takahashi, Synth. Met. **103**, 1907 (1999).
[15] M. Tamura, K. Yakushi, H. Kuroda, A. Kobayashi, R. Kato, and H. Kobayashi, J. Phys. Soc. Jpn. **57**, 3239 (1988).
[16] H. Seo, J. Phys. Soc. Jpn. **69**, 805 (2000).
[17] H. Seo and H. Fukuyama, J. Phys. Soc. Jpn. **66**, 1249 (1997).
[18] H. Tajima, K. Yakushi, H. Kuroda, and G. Saito, Solid State Commun. **56**, 159 (1985).
[19] H. Tajima, M. Tamura, H. Kuroda, T. Mori, and H. Inokuchi, Bull. Chem. Soc. Jpn. **63**, 538 (1990).
[20] R. Chiba, H. Yamamoto, K. Hiraki, T. Takahashi, and T. Nakamura (private communication).